CORONAL DIAGNOSTIC SPECTROMETER
SoHO

CDS SOFTWARE NOTE No. 13

Version 1.2 18 May 1994

# PRELIMINARY REPORT ON THE CALIBRATION OF THE VDS FLIGHT DETECTOR

W. Thompson
NASA Goddard Space Flight Center
Laboratory for Astronomy and Solar Physics
Code 682.1
Greenbelt, MD 20771, USA

thompson@serts.gsfc.nasa.gov
pal::thompson

Table 1: Detector quantum efficiency as a function of wavelength.

| $\lambda$ (nm) | Q.E. (%) |
|---|---|
| 30.41 | 18.98 ± 0.32 |
| 36.11 | 14.43 ± 0.76 |
| 40.51 | 17.22 ± 0.25 |
| 49.01 | 16.11 ± 0.26 |
| 58.41 | 13.23 ± 0.22 |
| 67.11 | 13.73 ± 0.58 |
| 92.01 | 9.56 ± 0.75 |
| 121.61 | 1.63 ± 0.20 |

# 1 Overview

The calibration of the VDS engineering model (EM) detector has been described previously [1]. The flight detector was calibrated in the same way, except for the following changes:

1. The photomultiplier tubes used to monitor the Krypton lamps were operated in a current measuring photodiode mode between the photocathode and the first amplification stage. This gave a steadier and much more repeatable measurement than the pulse counting mode used during the engineering model calibration.

2. Additional linearity tests were performed by placing a piece of frosted magnesium flouride ($MgF_2$) just in front of the lamp. This acted as a diffuser, and made the image pattern seen by the detector invariant relative to the aperture used. However, it also greatly decreased the amount of light falling on the detector. Tests were also done without the diffuser in place, replicating the test done with the engineering model detector.

Some things still need to be done before the calibration can be considered to be complete. In particular, the transmission of the $MgF_2$ window used to protect the microchannel-plate (MCP) needs to be measured. This quantity was measured as 18.5% transmission for the window used for the engineering model detector, and we have applied that number for the flight detector. It will be remeasured when the $MgF_2$ window currently on the flight detector is returned to Goddard.

# 2 Photometric calibration

## 2.1 Quantum Efficiency

The absolute quantum efficiency of the VDS detector is controlled by the microchannel-plate wafer within the Image Intensifier and Converter (IIC) section of the detector. The quantum efficience of the MCP was measured by O. H. W. Siegmund at the University of California Space Sciences Laboratory before delivery to Goddard. The measured results are shown in Table 1. The quantum efficiency in the wavelength region of interest, 30–65 nm ranges from 13–19%. The low quantum

Table 2: CCD offset values for the individual readout quadrants.

| Quadrant | Average Offset (ADC/pixel) |
|---|---|
| A | 217.94 |
| B | 207.47 |
| C | 182.08 |
| D | 179.29 |

efficiency at the Lyman-$\alpha$ line at 121.61 nm is desirable to reduce the effect of any scattered radiation inside the spectrograph.

### 2.2 CCD offsets

Each CCD quadrant has a separate offset value associated with it. Thus, the data values are guaranteed to be positive. Table 2 shows the average offsets for each quadrant. However, it was found that the offsets could drift between extremes that were 8 ADC/pixel apart, so that it is important to have a good value of the local background for each image. There was no indication that the offset value changed significantly during the readout of a single exposure; however, other effects such as scattering could also affect the local value of the background. The best way to determine the local background is to make the data extraction window around a spectral line wide enough to be able to measure the signal level just outside the line. However, this has to be confirmed with the detector installed within the CDS instrument.

### 2.3 Throughput

Tests of the VDS flight detector were done at programmable voltages of 0, 50, 100, 150, 200, 250 in the units used by the EGSE software, e.g.

VDS SETPROGVOL 15 $n$

These correspond to voltages across of the MCP of approximately 600V, 678V, 756V, 834V, 912V, and 990V. Table 3 gives the measurements we made, based on the housekeeping data, of the correspondence between the programmable voltage setting and the actual voltage across the MCP wafer.

We define the throughput of the detector as the number of Analog-to-Digital Conversion (ADC) "counts" for each photon that interacts with the MCP. In essence, this is a measure of the amplification of the detector. The total number of ADC units is proportional to the Q.E. times the throughput. Measuring the throughput requires calibrating the input radiation, which was done with a NIST photodiode, and adjusting for the MCP quantum efficiency, and the $MgF_2$ window transparency. Since some factors are provisional (see Section 1), the results are only preliminary.

The throughput was measured in two ways. One method involved putting the Krypton lamp $\sim$2 m away from the detector, and allowing the light to fall on the face of the detector without any intervening optics. The other method used two off-axis parabolic mirrors to refocus the radiation

Table 3: Correspondence between programmable voltage #15 and MCP voltage

| Programmable voltage #15 | MCP voltage |
|---|---|
| 0 | 602.908 |
| 25 | 639.109 |
| 50 | 678.140 |
| 75 | 717.171 |
| 100 | 756.202 |
| 125 | 795.231 |
| 150 | 834.167 |
| 175 | 873.198 |
| 200 | 912.326 |
| 225 | 951.357 |
| 250 | 990.486 |
| 255 | 998.292 |

Table 4: Detector throughput as a function of MCP voltage.

| Voltage | Throughput (ADC/photon-event) |
|---|---|
| 600 | 0.240 |
| 678 | 0.767 |
| 756 | 2.27 |
| 834 | 6.25 |
| 912 | 14.3 |
| 990 | 32.7 |

on the detector. The first method depends on the amount of radiation per unit area, while the second depends on the total amount of light. Each gave similar results, within the expected errors of the technique. The average results are shown in Table 4. Thus, if one wants to tune the VDS detector such that one photon event results in one ADC "count", then the voltage should be set somewhere between 678V and 756V.

The VDS detector uses electronic shuttering. The voltage on the MCP is switched between the desired voltage during integration and a rest voltage between integrations. The rest voltage of the VDS flight detector was measured as 331V. Although no measurements of the VDS sensitivity were made with the MCP shuttered off, one can extrapolate the curve in Table 4 and estimate that the "off" sensitivity of the VDS detector is $\lesssim 0.005$ ADC/photon-event.

### 2.4 Exposure time accuracy

The VDS detector is electronically shuttered by raising and lowering the voltage on the MCP wafer. There is a rise and a decay time associated with this process. When taking an image, this rise and decay time appears as an additional amount of effective exposure time, i.e. $T_{\rm eff} = T_{\rm exp} + \Delta T$.

Figure 1: Plots of system response versus exposure time, for three MCP voltages. Also shown are least-square fits to determine the decay constants shown in Table 5.

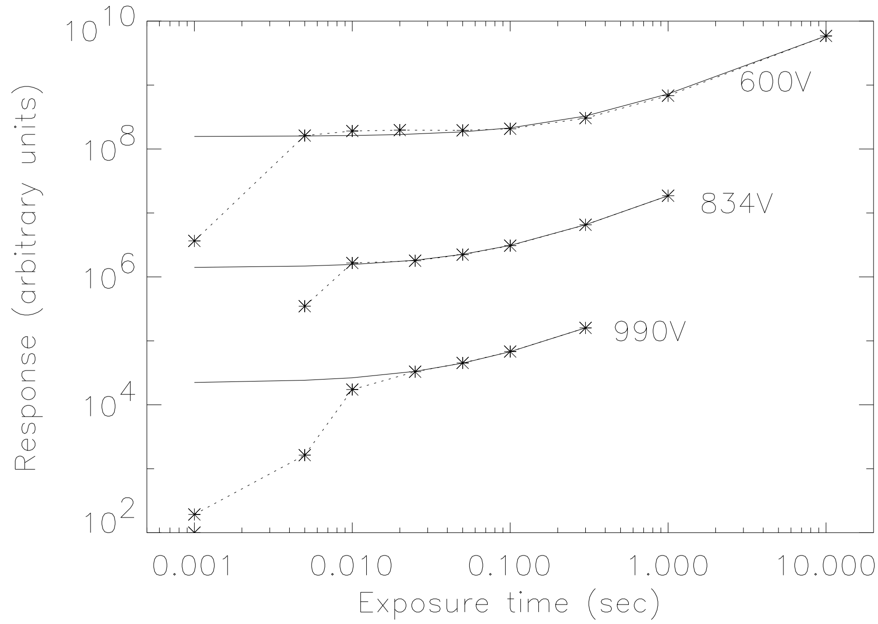


Table 5: Effective decay times as a function of voltage.

| Voltage | Effective Decay Time (ms) |
|---|---|
| 600 | 274.4 |
| 834 | 81.0 |
| 990 | 47.6 |

These effective decay times were determined by comparing the brightness of images taken at a variety of exposure times. The results are shown in Figure 1 and in Table 5. Also evident from Figure 1 is that when the exposure time is low enough, ranging from 5–20 ms depending on the voltage setting, the MCP voltage never has enough time to come to its stable value.

## 2.5 Linearity

The linearity of the VDS detector was measured by placing a series of calibrated apertures in the collimated beam between the two detectors. The resulting images were compared to a reference image taken with the smallest aperture and the lowest operating voltage, to ensure that this reference image was taken under linear conditions. This test was performed in two ways: with a diffuser in front of the lamp, and without.

The results of the linearity measurements without the diffuser are shown in Figure 2. One effect that had to be taken into account is that as different apertures were placed in the beam, the depth of focus of the measurement system changed. After a certain point the lamp, which was placed

Figure 2: Plots of system linearity for various MCP voltages.

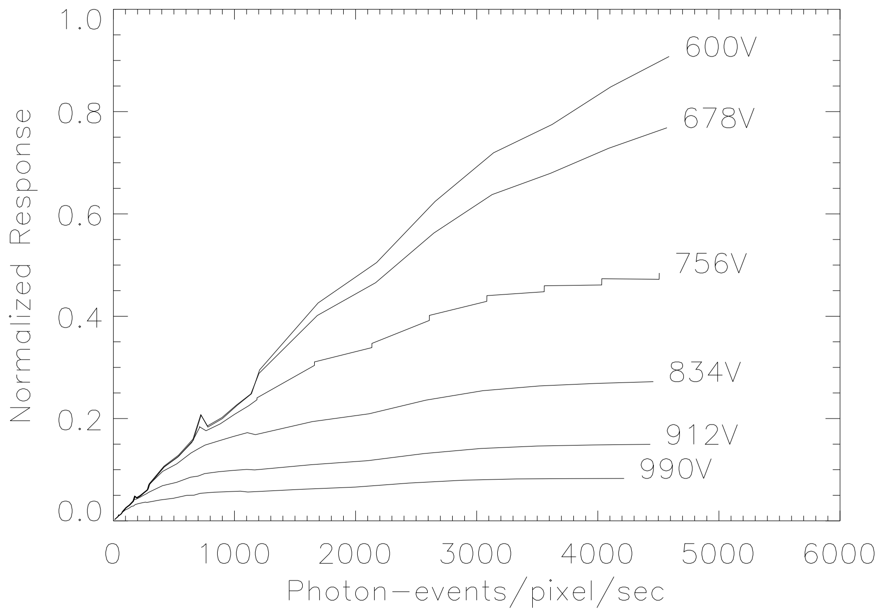


about an inch behind the focal plane, was essentially in focus. Thus, for the larger apertures, only the middle intensity values could be used, as they were not sensitive to the degree of focus of the lamp.

Some comment should be made about the differences between these curves and those reported for the engineering model detector [1]. First of all, in that earlier report the curves were given relative to the number of photons/pixel/sec impinging on the detector. Here the numbers are given in terms of the more useful photon-events/pixel/sec. These quantities differ by the MCP quantum efficiency at 123.6 nm, which is ~0.0163.

However, given that, it is evident that these data show more non-linearity than that reported for the engineering model detector. When the EM detector was measured, there was a problem with monitoring the lamp [1], such that the actual lamp brightness was uncertain by as much as a factor of two. To overcome this problem, the different segments that made up the total linearity curve were pieced together by hand. In other words, guesses were made about how far off the lamp monitor was. It is possible that this procedure introduced some error in the linearity curves. No such correction needed to be made for the flight detector data.

It was found that if one multiplied the number of photon-events/pixel/sec by the throughput given in Table 4, thus generating the predicted number of ADC/pixel/sec if the detector were linear, then the curves for all the MCP voltages merge into a single curve. This is shown in Figure 3

We were able to successfully fit the non-linearity characteristics of the detector using the function:

$$F = \frac{R + (R/R_0)^P}{T} \tag{1}$$

where $F$ is the number of photon-events/pixel/sec, $R$ is the system response in ADC/pixel/sec, and $T$ is the throughput from Table 4. The fitted parameters are $R_0 = 904.0$ and $P = 4.1945$. This

Figure 3: Detector linearity characteristics with system throughput taken into account. Data from all MCP voltages used are included. Also shown is a least-square fit to the data. See text for details.

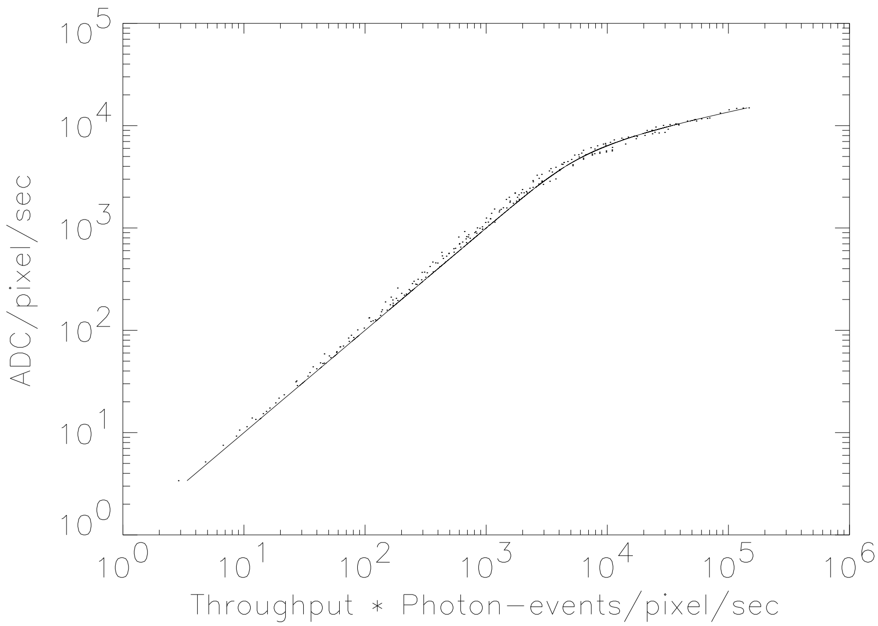


fitted curve is shown in Figure 3.

We also did linearity tests with a frosted $MgF_2$ diffuser in front of the lamp. These measurements only went out to about 100 photon-events/pixel/sec, and showed that the detector acted linearly within this range at all voltage settings.

### 2.6 Flat-field response

The flat field response of the VDS detector was measured by illuminating the detector with a lamp placed $\sim$2 meters away. The light was allowed to fall directly onto the detector with no intervening optics. A series of apertures could be placed in front of the lamp to control the amount of illumination. Measurements were made with the detector in three different positions in the beam, to remove any artifacts caused by the illumination pattern.

A typical flat-field pattern is shown in Figure 4. This image was produced by averaging together images taken at the three different test positions, rejecting any pixels that were significantly different from the corresponding pixels of the other two images. This greatly reduces the effects of artifacts in the input illumination caused by the light having to pass through the $MgF_2$ window. Note that each quadrant has a slightly different amplifier gain in the CCD electronics. The box drawn on the image shows the part of the detector that will be used during flight. Table 6 gives the percent RMS deviations from perfect flatness for the data in this box as a function of MCP voltage and CCD quadrant.

When the IIC is operated past its linear regime, the flat field characteristics of the detector change. This is illustrated in Figure 5. Two hexagonal structures can be seen in this image. The

Figure 4: Flat field pattern of the VDS detector. The image intensity has been stretched to enhance the contrast. The box illustrates the part of the detector that will be used during flight. The percent RMS deviations for the data in this box are given in Table 6.

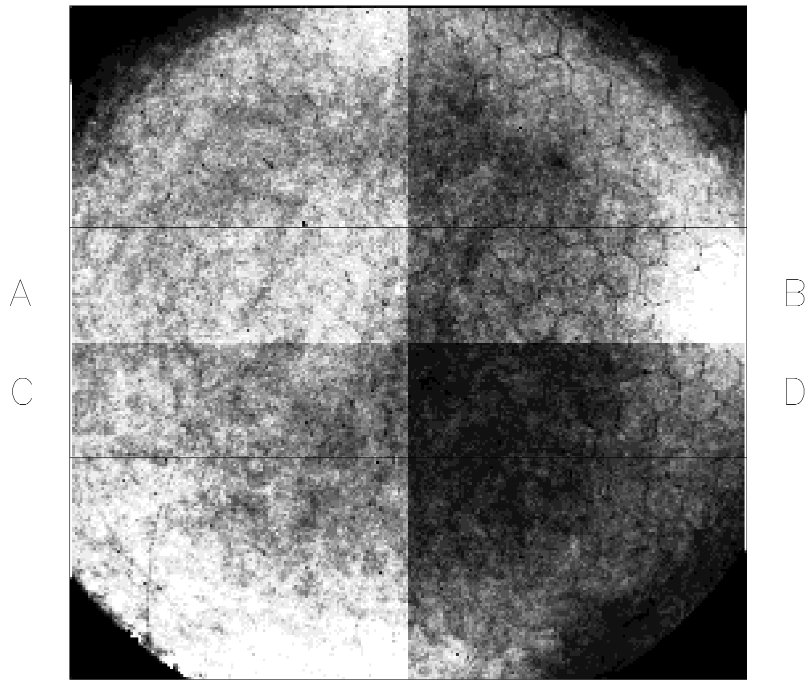


Table 6: Percent RMS deviations for the portion of the VDS detector that will be used during flight, as a function of CCD quadrant and MCP voltage.

| | Quadrant | | | |
|---|---|---|---|---|
| Voltage | A | B | C | D |
| 600 | 6.1 | 10.2 | 6.9 | 9.0 |
| 678 | 5.3 | 9.6 | 6.0 | 8.2 |
| 756 | 6.1 | 9.5 | 6.7 | 8.6 |
| 834 | 7.1 | 10.2 | 7.6 | 9.4 |
| 912 | 7.9 | 12.0 | 8.3 | 10.7 |
| 990 | 8.3 | 12.7 | 8.3 | 11.3 |

Figure 5: Blowup of part of the flat-field pattern of the VDS detector operated beyond its linear regime. The image intensities have been stretched to enhance the contrast.

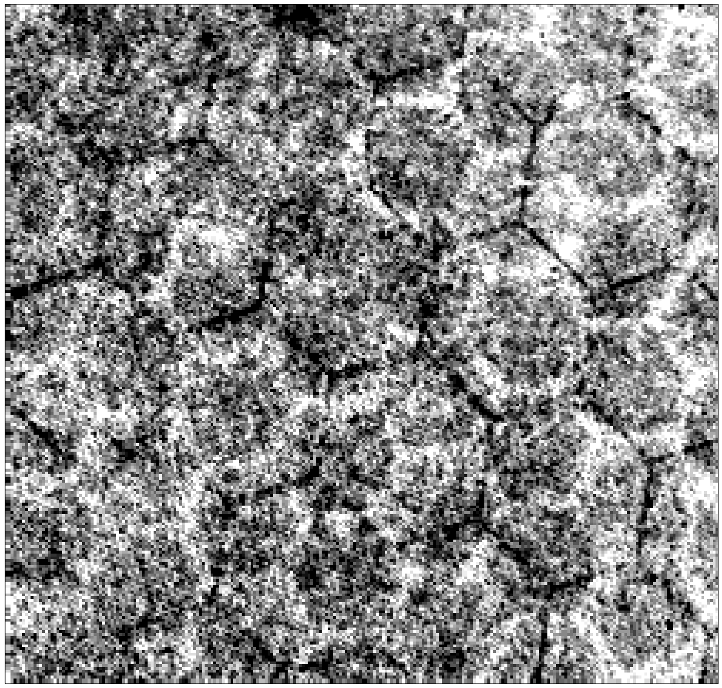

larger hexagons outlined in thin dark lines are due to the fiber optic faceplate at the back of the IIC. The somewhat smaller hexagonal pattern outlined in more diffuse bright lines come from the MCP wafer. They are much less evident when the detector is operated within its linear regime. We have been able to model this by allowing the factor $R_0$ in equation 1 to vary as a function of position.

# 3 Resolution

The limiting resolution due to the Nyquist frequency of the $21 \times 21$ CCD used in the VDS detector is 23.8 lp/mm. The VDS Flight detector is able to resolve standard Air Force resolution targets down to this limiting resolution, as can be seen in Figure 6. A square-wave modulation transfer function (MTF) derived from the image in Figure 6 is shown in Figure 7. Curves for both vertical and horizontal resolution are shown—they are very similar within the limits of the technique. The measurement was only taken out to a spatial frequency of $\sim$20 lp/mm as it was found to be difficult to estimate the value of the MTF at the Nyquist frequency from the data.

# 4 Dark current

Since the VDS detector is designed to work at a CCD temperature of -70 C, it has very low dark current characteristics. Also, since the MCP has no photocathode, it produces very few thermal electrons, even though it is uncooled. Table 7 gives the dark current characteristics of the VDS flight detector, determined by comparing images taken with the lamp off at long exposure times to

Figure 6: Image taken with the VDS detector of a standard Air Force 1951 resolution test target: (b) is a blow-up of (a) showing groups 4 and 5. The images have been stretched and contrast-enhanced to show detail.

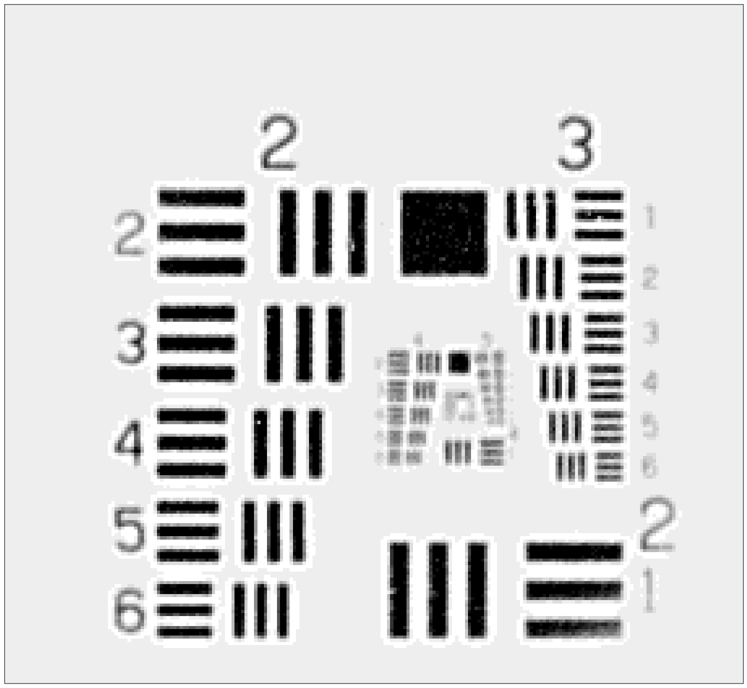


(a)

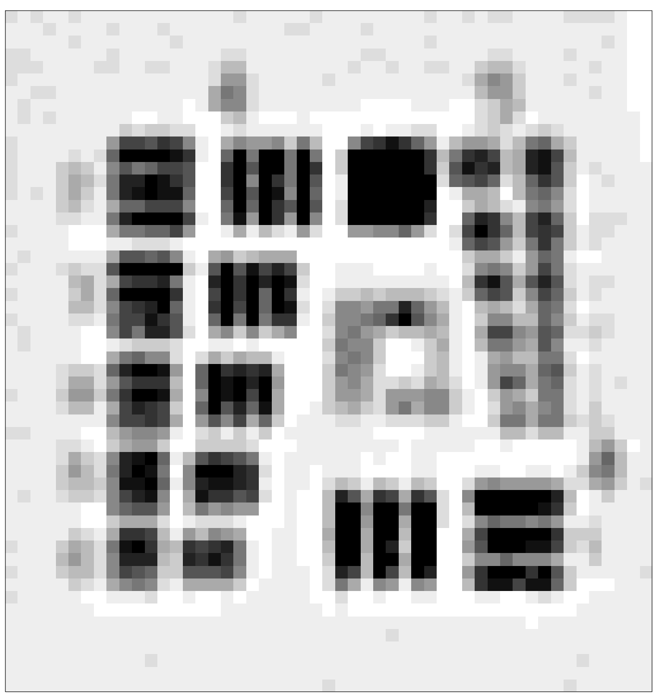

(b)

Figure 7: Square-wave modulation transfer function based on an image of an Air Force resolution target. The solid line represents the resolution in the horizontal direction, and the dashed line is for the vertical direction.

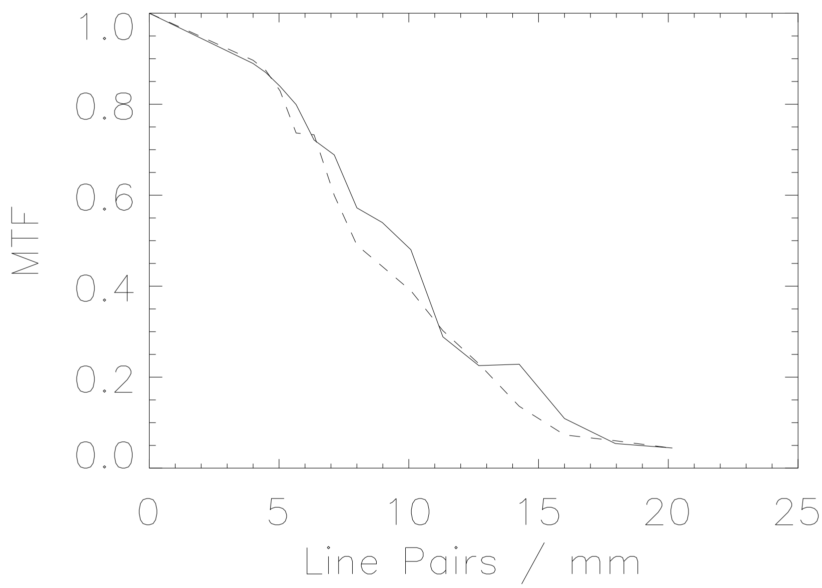


Table 7: Dark current characteristics of the VDS flight detector.

| MCP Voltage | Dark current (ADC/pixel/s) |
|---|---|
| 600 | 0.0039 |
| 990 | 0.011 |

those taken at short exposure times. However, these numbers are uncertain, since the effect was so small.

# 5 Noise

## 5.1 Readout noise

The readout noise characteristics of the detector depend to some extent on the electromagnetic environment in which it sits. Typically there was an RMS deviation of 1.5–2 ADC/pixel. However, there was electromagnetic interference from the ground support equipment picked up in some of the (non-flight) cabling external to the vacuum tank, which caused the RMS deviation in quadrant C (and occasionally A) to be elevated to approximately 5.5 ADC/pixel. It was determined that this effect could be neutralized by moving and/or shielding the cables, which resulted in the readout noise determinations shown in Table 8.

Table 8: Readout noise for the four CCD quadrants.

| Quadrant | RMS deviation (ADC/pixel) |
|---|---|
| A | 1.67 |
| B | 1.52 |
| C | 1.88 |
| D | 1.41 |

Figure 8: Statistical variation based on a pixel-by-pixel analysis of sequential images.

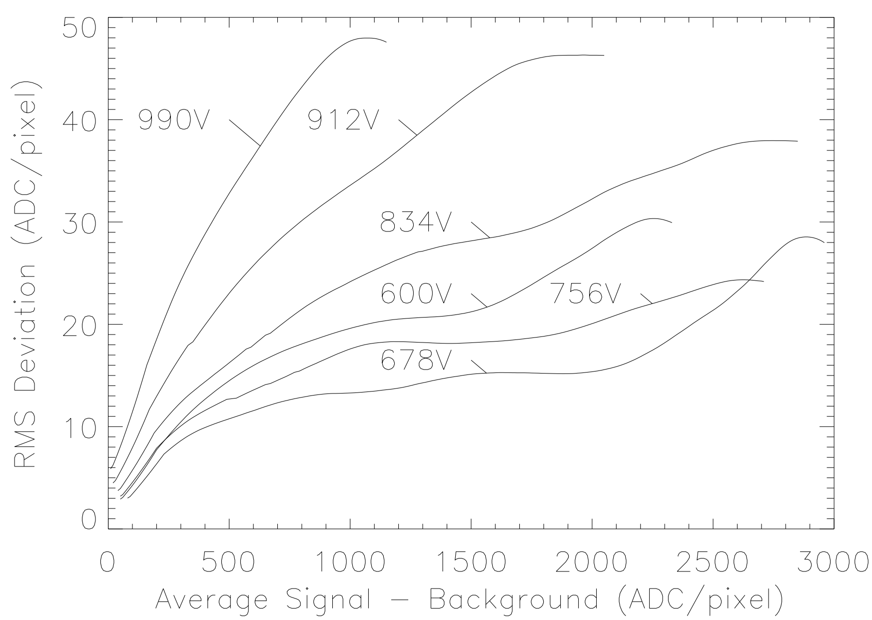


## 5.2 Statistical Variation

The dominant sources of noise in the VDS detector are the Poisson statistics inherit in the photons themselves, and the "shot" noise produced within the image intensifier. This latter term represents the amount of variability in the amplification process, also known as the pulse height distribution, which is a strong function of the voltage across the MCP. For a given MCP voltage, both the Poisson statistics and the shot noise should be proportional to the square root of the number of photons collected.

To measure the dark current, a series of five images were taken as rapidly as possible. This procedure was repeated for different MCP voltages, and for different intensity levels. Care was taken to ensure that the intensity levels were within the linear range of the detector for the current MCP voltage.

From each series of five images a mean and standard deviation were calculated for each CCD pixel. The results are illustrated by the curves in Figure 8. However, a careful examination of Figure 8 together with the information in Table 4 reveals that the measured RMS deviations are actually smaller than Poisson statistics predict they should be for all but the 600V trace, by as much as a factor of $\sim$4 for the larger MCP voltages. There are two possible reasons why this may be:

1. The absolute calibration of the VDS detector, represented by Table 4, could be off. This may be either because the NIST photodiode is less sensitive than supposed, or because the $MgF_2$ window is more transparent than assumed. Additional measurements on these components of the test setup should allow us to determine whether either or both of these is the case.

2. Some property of the VDS detector acts to suppress the variability of any individual pixel.

One possible effect that could produce the effect discussed in the second item above is the resolution of the VDS detector. The effect of the IIC and lens sections of the detector is such that each detected photon produces a "splash" of light on the CCD. This splash has a full-width half-maximum of $\sim$30 $\mu$m, which is somewhat larger than the CCD pixel size of 21 $\mu$m. Thus, each pixel is affected to some degree by the pixels surrounding it. To determine whether or not this could explain the discrepency, we did Monte Carlo simulations of the VDS detector, and found that the RMS deviation of this simulated data was indeed suppressed by about a factor of two.

We then attempted to recover the true statistical properties of the image by adding together bins of pixels, of sizes $4 \times 4$, $8 \times 8$ and $16 \times 16$. We theorized that these "superpixels" would be largely shielded from the effect discussed above. This appeared to be successful with the simulated data, which was suppressed by only 20% relative to Poisson statistics when compressed by 4 in both dimensions. When applied to the VDS data, it appeared that convergence was achieved when the compression factor was 8, and increasing this to 16 had no additional effect. Figure 9 shows the result of the $8 \times 8$ compression, with the resulting averages divided by 64, and the standard deviations divided by 8 (i.e. we made the assumption that the deviations scale as $\sqrt{N}$) so that a direct comparison can be made with Figure 8.

The traces for MCP voltages 600V and 678V do not appear in Figure 9 because it was discovered that an additional effect was contributing to the statistics of those images. Examination of the image totals demonstrated that there was an overall brightness change from image to image at 600V and 678V that wasn't present in the images taken with higher MCP voltages. Two possible causes were examined: either the CCD offset was changing when these images were made, or the IIC amplification was changing. Since the statistical properties of these effects are global rather than local, they are not amenable to the pixel-summing procedure outlined above.

Further examination of the images led to the conclusion that the amplification was changing. Table 9 gives the estimated RMS stability of the VDS detector as a function of MCP voltage. The value for 990V seemed to be dominated by the low level of light during the test, rather than an intrinsic property, so it is not reported here.

# 6 Scattered Light

The scattered light characteristics of the VDS detector were measured in two different ways—as light scattered into small distances from the image, and light scattered into a diffuse background.

Figure 9: Derived statistical variation based on sums of $8 \times 8$ pixels. See text for details. The resulting averages are divided by 64, and the standard deviations are divided by 8 so that a direct comparison can be made with Figure 8.

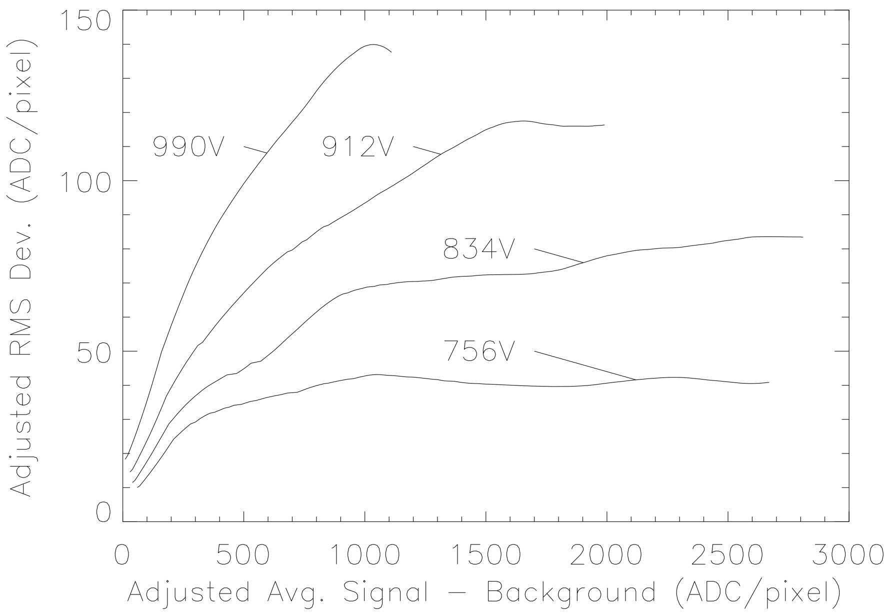


Table 9: Estimated root-mean-square stability of the VDS throughput, in percent.

| Voltage | Stability |
|---|---|
| 600 | 1.26 |
| 678 | 0.39 |
| 756 | 0.055 |
| 834 | 0.083 |
| 912 | 0.088 |

Figure 10: Scattered light measurements displayed as line-spread functions. The dashed line is taken from measurements around hot spots on the engineering model MCP (see text). The solid represents the measurements based on imaging a slit onto the detector, and is contaminated by scattering within the $MgF_2$ protective faceplate. The plots are normalized to unity at the origin—the solid line exhibits saturation in the CCD.

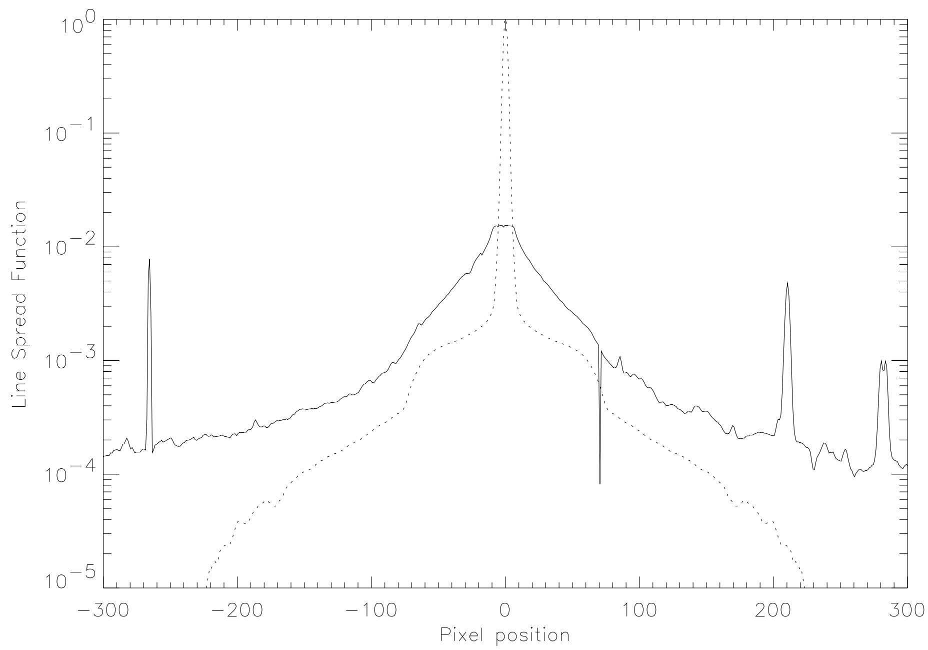


## 6.1 Small angle scattered light

The amount of light scattered into a small area around a feature was measured using the engineering model detector [1]. The measurement was based on light generated from small scratches on the front surface on the MCP, which is why the test could not be duplicated with the flight detector. Attempts to measure the scattering using slit and pinhole images turned out to be dominated by scattering within the test apparatus.

The measurements showed that a spectral line image would produce scattered light at the level of $\sim 10^{-3}$ of the line's peak intensity, out to a distance of ~60 pixels. This is shown in Figure 10, which is reproduced from the engineering model report [1].

## 6.2 Large angle scattered light

The diffuse background produced by scattered light within the VDS detector was measured by looking at the brightness of the image corners outside of the IIC active area when the entire VDS was illuminated. This brightness was about 13% of the brightness of the image itself, most of which cannot be accounted for by the small angle effect discussed above. If one divides by the total number of pixels contributing to this diffuse background, one comes to the conclusion that the amount of scattered light in any one pixel is proportional to $1–2 \times 10^{-7}$ of the total signal measured in all the pixels taken together. It is felt that this represents scattered light within the section of the detector between the IIC and the lens.

# 7 Conclusions

## 7.1 Dynamic Range

The full well capacity of the Tektronix CCDs used in the VDS detector were typically about 150,000 $e^-$. However, the actual upper limit on the data returned from the flight detector was imposed by the 12 bit A/D converter, which had an upper limit somewhat below the CCD full well capacity. Combining this information with the data on readout noise (Table 8), one obtains that the dynamic range of the VDS flight detector in a single exposure is ~2000:1. A greater dynamic range can be achieved by taking multiple images with different exposure times.

## 7.2 Photometric calibration

Converting an image taken with the VDS detector into a photometric flux is a multistep process. First, the local background must be estimated and subtracted from the data. Next, the linear flat field response must be removed from the image (Figure 4). After that, the exposure time must be adjusted to take into account the rise and decay times of the electronic shutter (Table 5), and convert the image into ADC/pixel/sec. At this point a correction can be made for the effects of non-linearity, using equation 1 with $T$ taken from Table 4, $P = 4.1945$, and $R_0$ being a function of position. After that the detector quantum efficiency (Table 1) and the efficiency of the CDS optics can be taken into account.

Figure 11 shows this procedure applied to one of the lamp images taken during calibration. The raw image (a) displays all the effects discussed above, including nonlinearity inducing a honeycomb pattern onto the image. The processed image (b) shows that these effects can be calibrated out to show what the actual lamp pattern looks like.

# References


[1] W. T. Thompson, A. I. Poland, O. H. Siegmund, M. Swartz, D. B. Leviton, and L. J. Payne. Measurements of an intensified CCD detector for the Solar Heliospheric Observatory. *SPIE*, 1743:464, 1992.

Figure 11: Image taken with the VDS detector of the illumination pattern of the Krypton resonance lamp used during the calibration tests. Image (a) shows the raw image taken by the detector. Image (b) shows the same image after the calibration process had been applied. The intensities have been stretched to show detail.

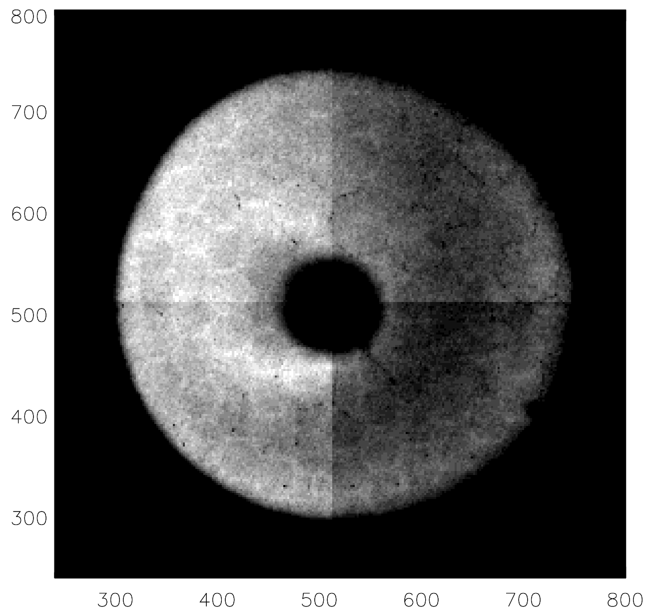


(a)

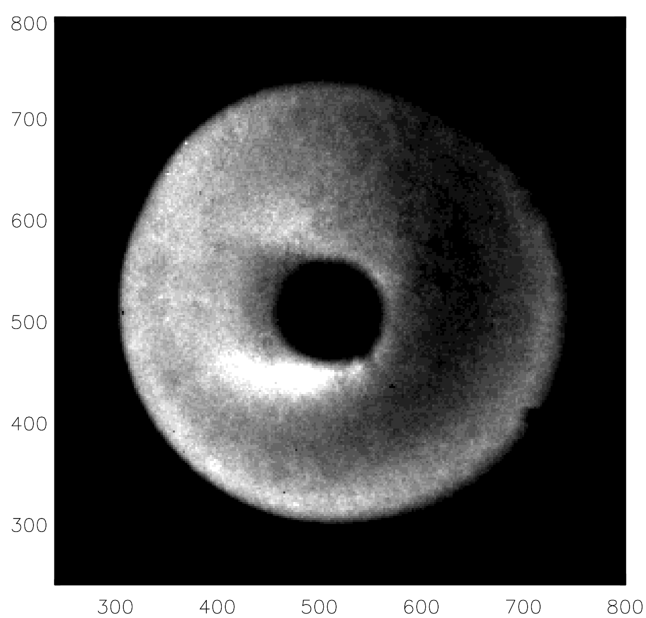


(b)